Comparisons of Scalar and Tensor Circularly-Polarized Holographic Artificial Impedance Surfaces

Yao, Ming; Mei, Peng; Pedersen, Gert Frølund; Zhang, Shuai

Published in:
The 16th European Conference on Antennas and Propagation (EuCAP)

DOI (link to publication from Publisher):
10.23919/EuCAP53622.2022.9769042

Publication date:
2022

Document Version
Accepted author manuscript, peer reviewed version

Comparisons of Scalar and Tensor Circularly-Polarized Holographic Artificial Impedance Surfaces

Ming Yao[1], Peng Mei[1], Gert Frølund Pedersen[1], Shuai Zhang[1]

[1] Antennas, Propagation, and Millimeter-Wave Systems (APMS) section, Department of Electronic Systems, Aalborg University, Aalborg, 9220, Denmark, mingya@es.aau.dk, mei@es.aau.dk, gfp@es.aau.dk, sz@es.aau.dk

***Abstract*— In principle, both scalar and tensor holographic artificial impedance surfaces (HAISs) can generate circularly-polarized waves. It is found, however, the previously-reported works on circularly-polarized holographic antennas are based on tensor impedance surfaces. This paper studies the generations of circularly-polarized waves by using scalar and tensor HAISs, and compare their performance in terms of design complexity, impedance bandwidth, 3-dB axial ratio (AR) bandwidth, realized gains, etc. The mechanisms of producing circularly-polarized waves using scalar and tensor HAISs are first formulated and presented. Two right-hand circularly-polarized holographic antennas are then implemented with the scalar and tensor HAISs, respectively, and simulated. The simulations conclude that the tensor HAIS indeed outperforms the scalar HAIS in generation of circularly-polarized waves. In particular, the peak gain of the tensor HAIS is much higher than that of the scalar HAIS. The conclusions obtained in this paper give a clear answer on designing circularly-polarized HAISs with good performance.**

***Index Terms*—scalar, tensor, holographic artificial impedance surface, circularly polarization.**

I. Introduction

The holographic artificial impedance surface (HAIS), a kind of sinusoidally-modulated reactant surface (SMRS) [1],[2], has attracted much interest in recent years since it features low profiles, high gain, and low cost [3]-[5]. The working mechanism of the HAIS combines the leaky wave theory, surface wave principle, artificial modulated surface concept, and holographic antennas technology [6]. According to the holography principle, an HAIS is regarded as a hologram that is constructed by two coherent waves (object and reference waves) [7]. When the HAIS is excited with the reference wave, it can radiate a kind of electromagnetic wave that perfectly matches the object wave. As a result, different types of HAISs have been designed according to the object waves with different properties. In 2010, Fong, *et al* proposed scalar (isotropic) and tensor (anisotropic) unit cells that could be fully employed to implement HAISs capable of radiating linearly-polarized (LP) and circularly-polarized (CP) waves, respectively [6].

Technically, it is essential to figure out the relationship between the effective surface impedance that scalar or tensor unit cell can offer and its dimension to design an HAIS. The main difference between scalar and tensor unit cells lies in the effective surface impedances which are scalar and tensor, respectively A scalar unit cell typically is geometrically symmetrical, while geometrical asymmetries should be introduced for a tensor unit cell such as square/circular patches with slots [8], [9], metallic strips [10], and rectangle patches [11] so that the tensor unit cell can generate arbitrarily polarized waves by modulating the currents and fields in any directions [6]. Due to the powerful properties of tensor unit cells, they have been widely employed to generate CP waves [9, 12, 13] and vertex waves with orbital angular momentum (OAM) modes [14], [15]. However, the CP and vertex waves can also be generated by using scalar HAISs when the target wave is a circularly-polarized one according to the holography principle [16]. To the best knowledge of the authors, no comparative studies on generation of CP waves using scalar and tensor HAISs have been reported. As a result, this paper gives comprehensive investigations and comparisons of CP scalar and tensor HAISs in terms of mechanism formulation, impedance bandwidth, 3-dB axial ratio (AR) bandwidth, realized gain, etc.

II. Design and Methodology

In this section, the mechanisms of generating right-hand circularly-polarized (RHCP) waves by using scalar and tensor HAISs are formulated.

Fig. 1 gives a schematic diagram of an HAIS, where the HAIS is mainly determined by the reference and object waves. The reference waves are typically generated with monopole antennas. For scalar and tensor HAISs, the reference and object waves are different. As a result, it is essential to figure out the specific expressions of reference and object waves, then the HAISs can be configured accordingly.

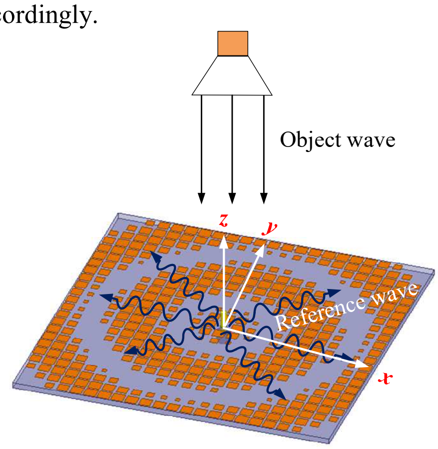

Fig. 1. Schematic diagram of the HAIS.

To generate CP waves, the expressions of the reference waves for scalar and tensor HAISs are given by:

$$\psi_{ref} = e^{-jk_t\rho} \tag{1a}$$

$$J_{ref} = (\frac{x}{\rho}\hat{x} + \frac{y}{\rho}\hat{y})e^{-jk_t\rho} \tag{1b}$$

where Ψ_{ref} in (1a) and J_{ref} in (1b) respectively correspond to the reference waves for scalar and tensor HAIS. k_t represents the transverse wave vector, and ρ is the radial distance from the monopole. From Eqs. (1a) and (1b), the expression of the reference wave for the tensor HAIS is a two-dimensional vector, while it is a scalar for the scalar HAIS. According to the holography principle, the object waves should be RHCP waves, and can be expressed as:

$$\psi_{obj} = e^{\begin{cases} -jk(x\cos\varphi + y\sin\varphi)\sin\theta + \arccos\frac{y}{\rho}, x>0 \\ -jk(x\cos\varphi + y\sin\varphi)\sin\theta + \arccos(2\pi - \frac{y}{\rho}), x\le 0 \end{cases}} \tag{2a}$$

$$E_{obj} = \begin{bmatrix} (-\sin\varphi + j\cos\theta\cos\varphi)\hat{x} + \\ (\cos\varphi + j\cos\theta\cos\varphi)\hat{y} - j\sin\theta\hat{z} \end{bmatrix} e^{-jk\rho} \tag{2b}$$

where Ψ_{obj} in (2a) and E_{obj} in (2b) respectively represent objective (RHCP) waves for scalar and tensor HAISs. φ and θ are azimuth angle and elevation angle. arccos(y/ρ) and 2π – arccos(y/ρ) are additional phases to realize right-hand circular polarization. On the other hand, the surface impedances of scalar and tensor HAISs are calculated by:

$$Z_{surf} = jZ_{ave} + M\,\mathrm{Re}\left(\psi_{obj}\psi^{*}_{ref}\right) \tag{3a}$$

$$\boldsymbol{Z}_{surf} = \begin{pmatrix} jZ_{xx} & jZ_{xy} \\ jZ_{yx} & jZ_{yy} \end{pmatrix} = \begin{pmatrix} jZ_{ave} & 0 \\ 0 & jZ_{ave} \end{pmatrix} + j\frac{M}{2}\mathrm{Im}\left(\boldsymbol{E}_{obj} \otimes \boldsymbol{J}^{\dagger}_{ref} - \boldsymbol{J}_{ref} \otimes \boldsymbol{E}^{\dagger}_{obj}\right) \tag{3b}$$

where Z_{surf} corresponds to the surface impedance. Z_{ave} denotes the average value of the surface impedance, and M is the modulation depth. '†' and '⊗' in (3b) represent Hermitian conjugation and Kronecker product.

Once the reference and object waves are determined, the desired surface impedances with respect to the position are needed to implement the scaler and tensor HAISs. Fig. 2 depicts scalar and tensor unit cells that have been widely used in designing HAISs. As is well known, the surface impedances of the scalar and tensor unit cells are closely associated with certain dimensions of the unit cells. The periodicities of the unit cells shown in Fig. 2 are 3 mm, the substrates are with a 1.5 mm thickness and a dielectric constant of 2.65, and the frequency of interest is selected as 17.5 GHz. For the scalar unit cell shown in Fig. 2(a), the surface impedance can be controlled by solely adjusting the gap g and the phase difference in x-direction as the scalar unit cell is perfectly geometric symmetry. After doing some simulations, the relationship between the surface impedance and parameter g can be fitted with a polynomial as following:

$$g = S_1 Z_{surf}{}^3 + S_2 Z_{surf}{}^2 + S_3 Z_{surf} + C_1 \tag{4}$$

where $S_1 = -3.05\times10^{-7}$, $S_2 = 3.14\times10^{-4}$, $S_3 = -1.12\times10^{-2}$, and C_1 = 13.83. While it is more complicated to determine the relationship for the tensor unit cell. We need to consider the components of Z_{xx}, Z_{yy}, and Z_{xy}, as well as g, θ_s, g_s, and phase differences both in x and y directions, as shown in Fig. 2(b). Here we fix g_s as 0.2 mm, the surface impedance with respect to the dimensions of the tensor unit cell can be calculated as [13]:

$$\theta_s = \theta_k\Big|_{z_{surf\_eff} = z_{surf\_eff\_max}} \tag{5a}$$

$$Z_{surf\_eff\_max} = 0.94g^{-3} - 12.7g^{-2} + 65.5g^{-1} + 107 \tag{5b}$$

where $Z_{surf\_eff\_max}$ is the maximum value of the Z_{surf_eff}, and Z_{surf_eff} is given by

$$Z_{surf\_eff} = j377\frac{A + \sqrt{B + C\cdot D}}{E} \tag{6a}$$

where

$$A = -j(377^2 + Z_{xx}Z_{yy} - Z_{xy}{}^2) \tag{6b}$$

$$B = -(377^2 + Z_{xx}Z_{yy} - Z_{xy}{}^2)^2 \tag{6c}$$

$$C = 4\times377^2\left[Z_{xx}\sin^2\theta_k - Z_{xy}\sin(2\theta_k) + Z_{yy}\cos^2\theta_k\right] \tag{6d}$$

$$D = Z_{xx}\cos^2\theta_k + Z_{xy}\sin(2\theta_k) + Z_{yy}\sin^2\theta_k \tag{6e}$$

$$E = 754\left[Z_{xx}\sin^2\theta_k - Z_{xy}\sin(2\theta_k) + Z_{yy}\cos^2\theta_k\right] \tag{6f}$$

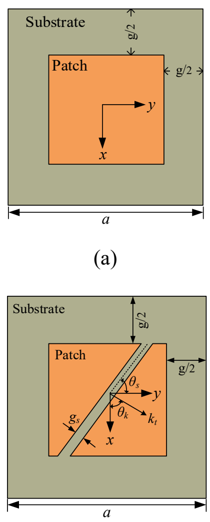

(b)

Fig. 2 Top view of (a) a scalar unit cell; and(b) tensor unit cell.

In Eq. (3a), the desired surface impedance for implementations of scalar and tensor HAISs also relies on Z_{ave} and M which are initially set as 175 Ω and 110, respectively. Therefore, the scalar HAIS can be constructed with (3a) and (4), while the tensor HAIS can be established by (3b), (5), and (6). The final patterns of the scalar and tensor HAIS are shown in Fig. 3. Comparing Fig. 3(a) and conventional scalar HAIS in Fig. 1, we can see the scalar HAIS can also conduct polarization modulation by changing the arrangement of unit cells. Here the scalar unit cells are placed with a counter-clockwise arrangement to realize RHCP waves. While the tensor HAIS realizes RHCP waves with the arrangement of unit cells, as well as directions of slots.

III. Results and Discussions

The performances of scalar and tensor RHCP HAISs are discussed in this section. The simulated reflection coefficients and AR with frequencies are shown in Figs. 4 and 5. Both scalar and tensor HAIS have good impedance match performances as seen in Fig.4, while the tensor HAIS can provide a wider AR bandwidth as observed in Fig. 5. The AR of tensor HAIS is 0.13 while the scalar HAIS is 1.34 at 17.5GHz. The realized gains of the scalar and tensor HAISs with frequencies are simulated and presented in Fig. 6, where it is observed that the peak gain for the tensor HAIS can reach 26.91 dBi while it is only 22.92 dBi for the scalar HAIS. The reason is that the scalar HAIS only utilizes LP wave in x-direction to generate the RHCP waves. While LP waves both in x and y directions are utilized for tensor HAIS. Therefore, the scalar HAIS loses the power of LP waves in y-direction. It can be demonstrated in the 3-dimensional radiation pattern as shown in Fig. 7. Compared with other directions, the beam width is wider at $\varphi = -45°$ in Fig. 7. It is caused by the polarization modulation for only LP waves in x-direction. In addition, the cross-polarization suppression level of scalar HAIS deteriorates at $\varphi = -45°$, as shown in Fig. 8 (c).

Performance comparisons of the scalar and tensor HAISs are displayed in table 1. From this table, the tensor HAIS has an AR bandwidth of 23% (14.74~20.4 GHz) and cross-polarization suppression level of 25.6 dB, while scalar HAIS is 19% (15.2~18.48 GHz) and only 7.7 dB respectively. Importantly, the peak gain for the tensor HAIS can reach 26.91 dBi while it is only 22.92 dBi for the scalar HAIS. Therefore, tensor HAIS provides much better performance with respect to scalar HAIS.

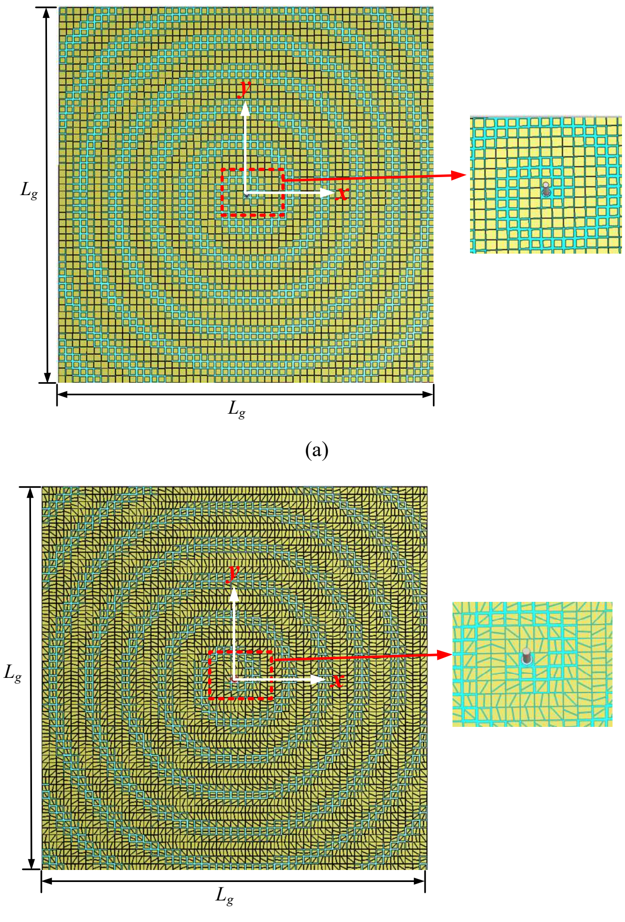

Fig. 3. Top view of (a) scalar RHCP HAIS; and (b) tensor RHCP HAIS.

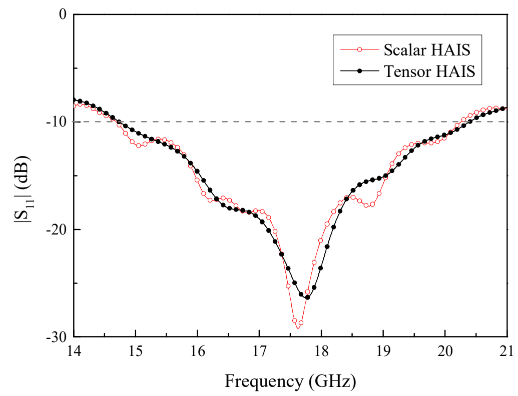

Fig. 4. S parameters for scalar and tensor RHCP HAIS.

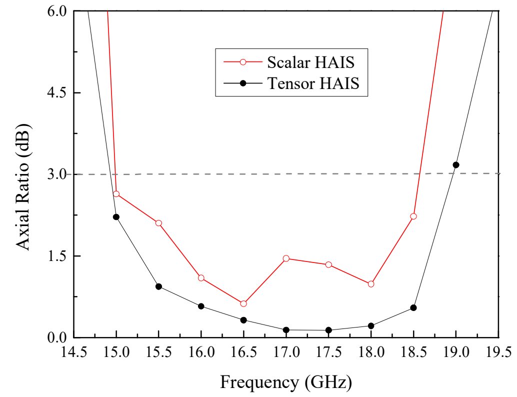

Fig. 5. Axial ratio for scalar and tensor RHCP HAIS.

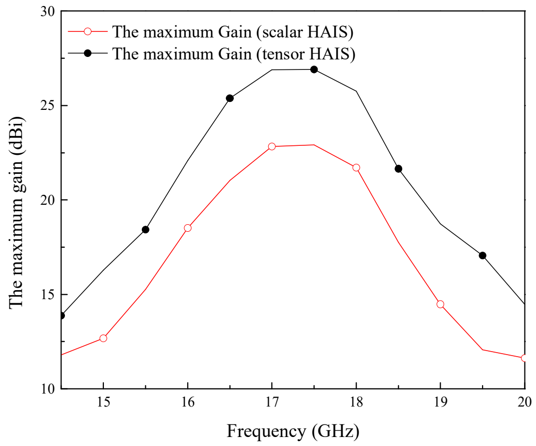

Fig. 6. Gain versus frequency.

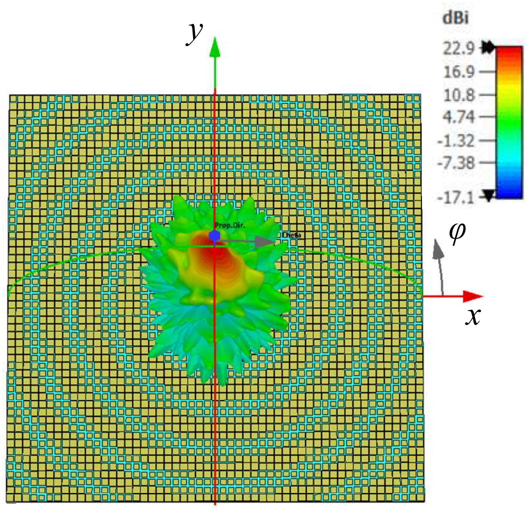

(a)

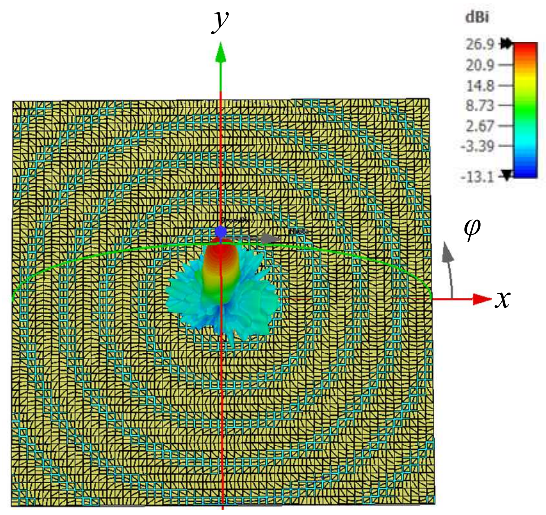

(b)

Fig. 7 3-dimensional radiation patterns at central frequency (a) of the scalar HAIS. (b) of the tensor HAIS.

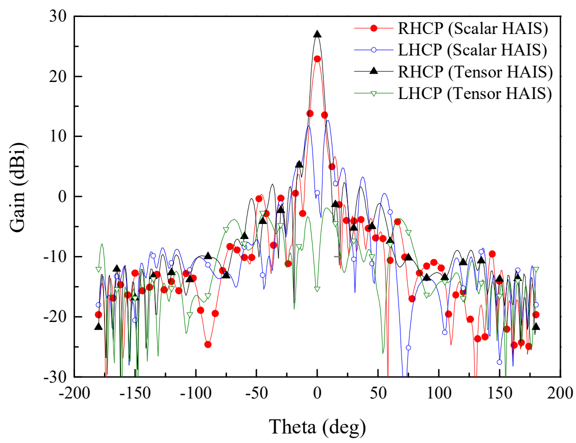

(a)

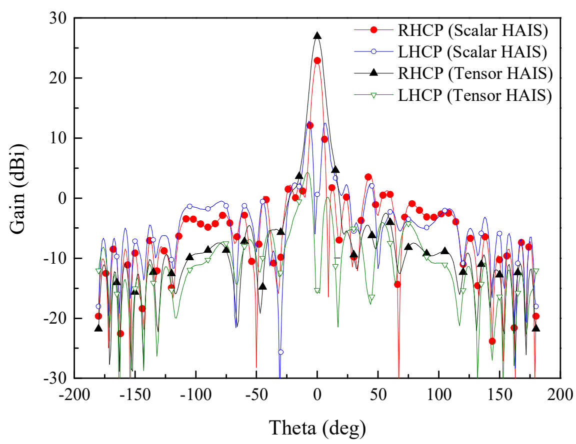

(b)

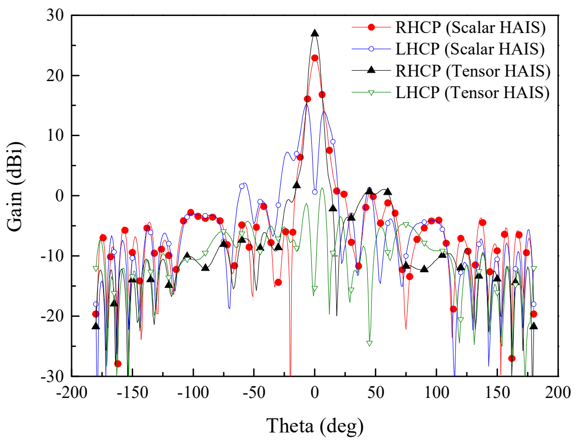

(c)

Fig. 8 Radiation pattern at central frequency. (a) φ = 0°. (b) φ = 45° (c) φ = –45° .

Table 1. Comparison of performances between scalar and tensor HAIS.

performances	Scalar HAIS	Tensor HAIS
Impedance	14.7~20.3GHz (32.9%)	14.74~20.4GHz (33.3%)
3-dB AR	15.2~18.48 (19%)	15~18.9 (23%)
Peak Gain	21.92 (dBi)	26.91 (dBi)
Cross-pol. Suppression	7.7 (dB)	25.6 (dB)

IV. CONCLUSIONS

In this paper, we present the mechanisms of producing circularly-polarized waves using scalar and tensor HAISs. And then we provide comprehensive investigations and comparisons of CP scalar and tensor HAISs in terms of mechanism formulation, impedance bandwidth, 3-dB AR bandwidth, realized gain, etc. The conclusions suggest that tensor HAIS provides much better performance, especially for peak gain, with respect to the scalar HAIS in generation of circularly-polarized waves.

REFERENCES

[1] A. M. Patel and A. Grbic, "A printed leaky-wave antenna based on a sinusoidally-modulated reactance surface," *IEEE Trans. Antennas Propag*., vol. 59, no. 6, pp. 2087-2096, Jun. 2011.

[2] A. Oliner, A. Hessel, "Guided Waves on Sinusoidally-Modulated Reactance Surfaces," *IRE Trans. Antennas Propag*., vol. 7, no. 5, pp. 201-208, 1959

[3] A. Amini and H. Oraizi, "High Gain Arbitrarily-Oriented Linearly-Polarized Leaky-Wave Antenna by Tensorial Impedance Surfaces," *2020 50th European Microwave Conference (EuMC)*, pp. 764-767, 2021

[4] Y. Li, H. Li, H. Wang, and T. Cui, "Wavelength-dependent holographic impedance metasurfaces," *Opt. Express*, vol. 29, no. 11, pp. 17330-17342, 2021.

[5] K. V. Lemberg, A. N. Kosmynin, D. A. Stupnitsky, E. O. Grushevsky and I. V. Podshivalov, "Tunable Meta-Surface Antenna Array with Holographic Beamforming," *2020 7th All-Russian Microwave Conference (RMC)*, pp. 159-161, 2020.

[6] B. H. Fong, J. S. Colburn, J. J. Ottusch, et al, "Scalar and Tensor Holographic Artificial Impedance Surfaces," *IEEE Trans. Antennas Propag*., vol. 58, no. 10, 3212-3221, 2010.

[7] M. Yao and J. L. Li, "Beam reconfigurable holographic artificial impedance surface at terahertz band," *J. Phys. D. Appl. Phys*., vol. 52, no. 15, p. 155001, 2019

[8] G. Minatti et al., "Modulated Metasurface Antennas for Space: Synthesis, Analysis and Realizations," *IEEE Trans. Antennas Propag*., vol. 63, no. 4, pp. 1288-1300, 2015.

[9] Y. Shen, S. Xue, G. Dong, J. Yang, and S. Hu, "Multiplexing Tensor Holographic Metasurface with Surface Impedance Superposition for Manipulating Multibeams with Multimodes," *Adv. Opt. Mater*., p. 2101340, 2021

[10] L. Gan, W. Jiang, S. Gong, Q. Chen and X. Li, "A Low-Profile and High-Gain Circularly Polarized Antenna Based on Holographic Principle," *2018 Asia-Pacific Microwave Conference (APMC)*, pp. 1031-1033, 2018

[11] A. Amini, H. Oraizi, M. Hamedani, and A. Keivaan, "Wide-Band Polarization Control of Leaky Waves on Anisotropic Holograms," *Phys. Rev. Appl*., vol. 13, no. 1, p. 14038, 2020.

[12] X. Wan, T. Y. Chen, Q. Zhang, et al, "Manipulations of Dual Beams with Dual Polarizations by Full - Tensor Metasurface," *Adv. Opt. Mater*., vol. 4, no. 10, pp. 1567-1572, 2016

[13] M. Yao, J. L. Li, L. Xia, and S. S. Gao, "Wide dual-band dual-circularly polarized holographic metasurface," *J. Phys. D. Appl. Phys*., vol. 52, no. 42, p. 425001, 2019.

[14] X. Meng et al., "Launcher of high-order Bessel vortex beam carrying orbital angular momentum by designing anisotropic holographic metasurface," *Appl. Phys. Lett*., vol. 117, no. 24, p. 243503, 2020.

[15] X. Meng et al., "Generation of multiple beams carrying different orbital angular momentum modes based on anisotropic holographic metasurfaces in the radio-frequency domain," *Appl. Phys. Lett*., vol. 114, no. 9, p. 93504, 2019.

[16] L. Zhu, Y. Liu and Y. Jia, "A High-Gain Circularly-Polarized Holographic Antenna Based on Impedance-Modulated Surface," *2020 Cross Strait Radio Science & Wireless Technology Conference (CSRSWTC)*, pp. 1-3, 2020.